Near Infrared Hyperspectral Imaging of *Fusarium*- Damaged Oats (*Avena sativa* L.)

Selamawit Tekle[1],[2], Ingrid Måge[3], Vegard H. Segtnan[3], Åsmund Bjørnstad[1]

ABSTRACT

The feasibility of hyperspectral imaging (HSI) to detect deoxynivalenol (DON) content and *Fusarium* damage in single oat kernels was investigated. Hyperspectral images of oat kernels from a *Fusarium*-inoculated nursery were used after visual classification as asymptomatic, mildly damaged, and severely damaged. Uninoculated kernels were included as controls. The average spectrum from each kernel was paired with the reference DON value for the same kernel and a calibration model was fitted by partial least squares regression (PLSR). To correct for the skewed distribution of DON values and avoid nonlinearities in the model, the DON values were transformed as DON*= [log(DON)]^3. The model was optimized by cross-validation, and its prediction performance was validated by predicting DON* values for a separate set of validation kernels. The PLSR model and linear discriminant analysis (LDA) classification were further used on single-pixel spectra to investigate the spatial distribution of infection in the kernels. There were clear differences between the kernel classes. The first component separated the uninoculated/asymptomatic from the severely damaged kernels. Infected kernels showed higher intensities at 1920, 2070 and 2140 nm, while non-infected kernels were dominated by signals at 1420, 1620 and 1850 nm. The DON* value of the validation kernels were estimated using their average spectrum, and the correlation (R) between predicted and measured DON* was 0.8. Our

[1] Department of Plant Sciences, Norwegian University of Life Sciences, P. O. Box 5003, 1432 Ås, Norway
[2] Corresponding email: selag@nmbu.no
[3] Nofima AS, Osloveien 1, NO-1430 Ås, Norway

results show that HSI has great potential in detecting *Fusarium* damage and predicting DON in oats but it needs more work to develop a model for routine application.

Abbreviations

DON: Deoxynivalenol, FHB: Fusarium Head Blight, HSI: Hyperspectral Imaging, LDA: Linear Discriminant Analysis, NIR: Near Infrared, PCA: Principal Component Analysis, PLSR: Partial Least Squares Regression, VIS: Visible.

INTRODUCTION

Fusarium head blight (FHB) is one of the important diseases of cereals worldwide. The disease causes substantial yield and quality losses every year (Parry et al., 1995, McMullen et al., 1997). It results in light-weighted shriveled kernels with pink to brownish discoloration (McMullen et al., 1997). *Fusarium* spp. produce a wide array of toxins (Bottalico & Perrone, 2002) which are involved in isolate aggressiveness and species pathogenicity (Langevin et al., 2004). These toxins raise food and feed safety issues and impair animal production as they cause feed refusal, vomiting, and reduced weight gain in farm animals. They are also associated with various acute and chronic ailments in animals and humans (Bergsjø et al., 1993, D'Mello et al., 1999). Deoxynivalenol (DON) and its derivatives, mainly produced by *F. graminearum* and *F. culmorum,* are the most commonly encountered *Fusarium*-toxins in Europe (Bottalico & Perrone, 2002) and in Norwegian small grain cereals (Bernhoft et al., 2013). Among the small grain cereals produced in Norway, oats (*Avena sativa* L.) are the most frequently and highly DON-contaminated cereal species (Bernhoft et al., 2013).

Fusarium infection has a significant impact on grain quality. *Fusarium graminearum* infection in barley (*Hordeum vulgare* L.) results in significant reduction in germination and kernel plumpness (Schwarz et al., 2001). In wheat (*Triticum aestivum* L.), infection results in poor baking performance and flour color, reduced loaf volume, and weak dough properties (Dexter et al., 1996, Nightingale et al., 1999, Wang et al., 2005). Infection destroys starch granules, storage proteins, and cell walls (Bechtel et al., 1985, Wang et al., 2005). Wheat kernels infected with *F. culmorum* display damaged starch granules, complete or partial lack of the protein matrix and complete disappearance of the starchy endosperm under severe infection (Jackowiak et al., 2005).

Significant degradation of the endosperm protein and lower content of storage proteins in *F. avenaceum* and *F. graminearum*- infected wheat are also reported (Nightingale et al., 1999).

The level of fungal secondary metabolites in grains (such as DON) is very low compared to the major seed constituents. Conventional NIR spectroscopy is not very sensitive to such minor constituents (Gowen et al., 2007). Therefore, efforts to calibrate DON contamination in bulk samples using NIR spectroscopy must rely on major effects of the disease on grain constituents that are correlated with DON (Siuda et al., 2008, Tekle et al., 2013). Hyperspectral imaging (HSI) is a powerful non-destructive tool to detect contaminants in food and feed(Gowen et al., 2007, Feng & Sun, 2012). It has higher sensitivity to minor seed constituents than conventional NIR spectroscopy (Gowen et al., 2007) due to the local enhancement of constituent signals. It combines conventional imaging and spectroscopy to provide a three-way data matrix known as a hypercube made of two spatial (x, y) and one wavelength (z) dimensions. It is made of hundreds of single channel, grayscale images, each representing a single band of spectral wavelength (Gowen et al., 2007). This combination of spatial and spectral information enables building 'chemical maps' that show distribution of grain components in individual kernels (Feng & Sun, 2012, Williams et al., 2010). Powerful and efficient data processing methods, however, are required to extract useful information from such hyperspectral data (Feng & Sun, 2012).

Hyperspectral imaging has previously been used to classify kernels and kernel regions based on fungal damage and/ or DON contamination (Gowen et al., 2007, Polder et al., 2005, Williams et al., 2010). The technique has been adapted for detection of maize kernels and regions within each kernel that were infected by *F. verticillioides* (Williams et al., 2010). Others have used HSI to detect *Fusarium* damage in wheat (Delwiche et al., 2011, Shahin & Symons, 2011, Shahin & Symons, 2012). Visible-NIR HSI classified wheat kernels into sound and *Fusarium*-

damaged with an accuracy of 92% (Shahin & Symons, 2011). It was possible to further classify the *Fusarium*-damaged kernels as severely and mildly damaged with an accuracy of 86 %. Similar levels of accuracies were achieved by using only six selected wavelengths (484 nm, 567 nm, 684 nm, 817 nm, and 900 nm), (Shahin & Symons, 2011). An extended VIS-NIR (400-1000 /1000-1700) HSI was shown to discriminate between *Fusarium*-damaged and sound wheat kernels with an average accuracy of 95%. The spectral absorption near 1200 nm, which was tentatively attributed to ergosterol was found to be useful for classification (Delwiche et al., 2011).

The level of *Fusarium* damage and DON contamination varies widely within and among kernels in a given *Fusarium*-affected seed lot (Liu et al., 1997). We hypothesized that hyperspectral imaging could utilize this variation to develop a robust NIR calibration model and map the variation in individual kernels. The objectives of this experiment were i) to test the feasibility of hyperspectral imaging in classifying oat kernels based on *Fusarium* damage and DON level ii) to map DON contamination in single oat kernels, and iii) to develop a calibration model that integrates both *Fusarium* damage and DON contamination.

MATERIALS AND METHODS

Samples

A half kilogram sample of the oat cultivar 'Bessin' was obtained from a *Fusarium* inoculation trial conducted in 2012 at the Vollebekk Research Farm of the Norwegian University of Life Sciences. The bulk sample had a DON value of 6.8 ppm. Kernels were visually categorized as severely damaged (highly shriveled, light weighted kernels with brownish discoloration and pinkish-white mycelium on most of the kernel surface), mildly damaged (kernels with modest kernel fill and localized brownish discoloration and pinkish-white mycelium), and asymptomatic

(well filled kernels with no visible discoloration or mycelium). Clean seeds of the same cultivar from an uninoculated nursery were used as control. The kernels were assigned randomly to the calibration set (*n*= 4 categories x 31 kernels) or the validation set (*n*= 4 categories x 14 kernels) and for scanning microscopy (*n*= 4 categories x 10 kernels).

Hyperspectral imaging

Hyperspectral images were acquired using SWIR hyperspectral camera (Specim, Spectral Imaging Inc, Oulu, Finland) with a Mercury Cadmium Telluride (HgCdTe) detector. SpectralDAQ (Specim, Spectral Imaging Inc, Oulu, Finland) was used for image acquisition software. The images were obtained in the 1000-2500 nm wavelength range distributed in 256 channels. The images had a spatial resolution of 200µm. Image acquisition was set at 5 mm/s scanning speed, 5ms exposure time and a frame rate of 25HZ. The ventral and dorsal surfaces of 31 kernels representing the calibration set of each kernel category were scanned following the sample presentation shown in Figure 1A. The same was done on 14 kernels from each kernel category representing the validation set following the sample presentation shown in Figure 1B. Hyperspectral images of kernels comprising seven uninoculated, seven asymptomatic, seven mildly damaged and ten severely damaged kernels were taken following the sample presentation shown in Figure 5A. Kernels were directly placed on the black sample holder and a 99% reflecting white reference bar was included in each image.

Figure 1 comes here.

Analysis of hyperspectral images

All data analysis was done in MATLAB (Release 2013b, The MathWorks, Inc., Natick, Massachusetts), using the Image Processing Toolbox, Statistics toolbox and in-house routines for

Principal Component Analysis (PCA) and Partial Least Squares Regression (PLSR). The analysis of the images followed these steps:

1. Transformation of raw signal into percent reflectance

Every image contains a white and black reference, as shown in Figure 1. The reflectance spectrum R_{rc} in row r and column c was calculated as

$$R_{rc} = \frac{I_{raw,rc} - I_{black,c}}{I_{white,c} - I_{black,c}},$$

where $I_{raw,rc}$ is the raw signal of row r and column c, and $I_{black,c}$ and $I_{white,c}$ were the average black and white references of column c. By doing the calculations column wise, variations due to line scanning were accounted for.

2. Remove background

In order to separate kernels from background, a threshold rule based on differences in reflectance spectra was used. The threshold was set by visual inspection of the spectra.

3. Preprocess spectra

Reflectance spectra were transformed to absorbance, and normalized by standard normal variate (SNV) to remove scattering effects.

4. Multivariate data analysis based on average spectra for each kernel

The average spectrum from each kernel was paired with the reference DON value, and a calibration model based on 248 images ((4 ventral + 4 dorsal images) x 31 kernels representing each kernel

category) was fitted by PLS regression. The DON values were transformed as DON*= [log(DON)]^3 prior to analysis in order to obtain a more even distribution and avoid curvature in the prediction model. The model was optimized by full cross-validation, and the prediction performance was validated by predicting DON* values of 112 separate validation kernels ((4 ventral + 4 dorsal images) x 14 kernels representing each kernel category).

A linear discriminant analysis (LDA) classification model was built using the latent variables from the PLS model. Only uninoculated and severely damaged kernels were used to define the classification rule, in order to get a clear separation between infected and non-infected samples.

5. Application of pixel-level multivariate models

The PLSR model and LDA classification were used on single-pixel spectra to investigate the spatial distribution of *Fusarium* infection within the kernels.

Microscopy and DON analysis

Cross-sections and surfaces of hulled and dehulled kernels representing each kernel category were further studied under the scanning electron microscope, SEM (ZEISS EVO 50-EP Environmental Scanning Electron Microscope, Carl Zeiss AG, Germany) at the Imaging Centre of the Norwegian University of Life Sciences. Ten kernels representing each kernel category were used. Samples were dissected in the middle and near the embryo to study the effect of infection on the grain ultra structure. The samples were mounted on aluminum stubs with conductive carbon adhesive tabs and double coated with gold-palladium (SC7640 Auto/ manual high resolution sputter coater) before examination under the SEM operating at an accelerating voltage of 25 kV.

Kernels used in the hyperspectral imaging were sent to the University of Minnesota, Department of Plant Pathology for single-kernel DON analyses. Deoxynivalenol content was determined by gas chromatography coupled with mass spectrometry following the protocol described in Jiang et al. (2006). The weight of each kernel was documented prior to grinding and DON analysis.

RESULTS AND DISCUSSIONS

Microscopy, DON content and kernel weight

Fusarium infection results in shriveled and light weighted kernels contaminated with DON (Snijders & Perkowski, 1990, Parry et al., 1995). Visual symptoms generally correlate with the level of DON contamination, but asymptomatic kernels can also be contaminated with significant levels of toxins. Therefore, accuracy of visual assessment of *Fusarium* damage is limited, and integrating DON analysis with visual assessment is a more robust way of evaluating the disease. Our results show that deoxynivalenol content and kernel weight of the visually categorized kernels followed the expected general trend. The asymptomatic kernels had the highest mean kernel weight and the lowest mean DON content while the severely damaged kernels had the lowest mean kernel weight and the highest DON content. The mildly damaged kernels had DON content and kernel weight values between the asymptomatic and the severely damaged ones (Table 1). However, there were a few exceptions to this general trend. There were kernels with very low DON (0.48 ppm, for example) in the severely damaged kernels category while there were kernels in the asymptomatic kernels category with substantial DON (21.91 ppm, for example). These kernels were detected with a better accuracy using HSI than our visual inspection.

Table 1 comes here

The microscopic study showed that the uninoculated and the asymptomatic kernels to be plump and free of any fungal mycelia. The severely damaged kernels were shriveled and heavily colonized with *F. graminearum*. Dense mycelial growth on the hulls and on the caryopsis of the severely damaged kernels was frequently observed. Denser mycelia were observed near the crease of the severely damaged kernels (Figures. 2 and 3). The cross-sections of the uninoculated kernels revealed a well-formed aleurone layer and intact endosperm, while the severely damaged kernels had collapsed and highly colonized aleurone layer with partially digested endosperm structure (Figures 3 and 4). Damage to the seed coat and the aleurone layers were also observed in the mildly damaged kernels, but the inner endosperm structure was intact. Similar effects of infection were observed in wheat (Bechtel et al., 1985, Jackowiak et al., 2005). Hyphae of *F. culmorum* were most prevalent in the layers of the seed coat tissues but were much less prevalent in the endosperm tissues of damaged wheat kernels (Jackowiak et al., 2005). Another study reported the pericarp and the aleurone layer to be the most affected tissues in *F. graminearum* infected wheat (Bechtel et al., 1985).

Figure 2, 3 and 4 come here

Hyperspectral image analysis

The level and the range of DON contamination in ground bulk samples do not correspond to that of individual kernels. In this study, the bulk DON content of the sample used was 6.8 ppm while the DON level of the individual kernels ranged from non-detectable levels to 386.5 ppm (Table 1). In a previous study, we investigated the potential of conventional VIS-NIR spectroscopy to estimate DON content of *Fusarium*-inoculated oat genotypes. Spectra were taken and DON level was analyzed from bulk ground samples. One hundred sixty six samples with DON value ranging from 0.05 ppm to 28.1 ppm were used. It was possible to develop a calibration model

which can be used for rough screening of the genotypes (Tekle et al., 2013). However, we hypothesized that a better calibration model for DON and *Fusarium* damage could be developed if the wider variation in DON among individual kernels and the higher sensitivity of HSI were utilized.

The average kernel size across all images was 554 pixels, ranging from 345 to 567 pixels. The correlation between the number of pixels and the measured kernel weight was 0.72, showing that the pixel size is fairly representative for the actual size of the kernels. The PLSR model, using the average spectra and the DON* values as x and y variables, respectively, was optimized by full cross-validation, and a 5-component model was selected. The model had a R^2 of 0.75 and 0.71 for calibration and cross-validation, respectively. The model was able to describe the majority of the DON* variation, although the prediction was not very good. The first PLS component was the most dominant, describing 32.9% of the DON* variation and 70.5% of the spectral variation. The second PLS component described additional 8.2% of the DON* variation and 14.2% of the spectral variation. The PLS score plot of component 1 versus component 2 in Figure 5A shows that there is a systematic pattern due to kernel category. These first two components separate uninoculated and asymptomatic kernels from severely damaged kernels. The mildly damaged kernels are overlapping with the severely damaged and the asymptomatic kernels. This can be explained by the large variation in DON value of the mildly damaged kernels (Table 1).

The line in Figure 5A is the LDA discrimination line that separates uninoculated kernels from severely damaged kernels. This line is used to discriminate between non-infected and infected pixels in the validation images. The loadings for the first component are shown in Figure 5B. The main peaks representing positive changes associated with increased infection are seen at 1925 nm, 2070 nm and 2140 nm, while negative changes at 1400 nm, 1626 nm and 1850 nm

196 corresponded to non-infection. In a previous study, peaks centered at 1432 and 1924 nm classified
197 DON-contaminated samples into high-DON and low-DON classes. These peaks were attributed
198 to O-H bands of water (Tekle et al., 2013). In comparison, absorbance peaks for *F. verticillioides*-
199 infected maize kernels were observed at 1960 nm and 2100 nm and at 1450 nm 2300 nm and 2350
200 nm for non-infected kernels (Williams et al., 2010).

201 *Figure 5 comes here*

202 Figure 6 shows the image analysis performed on the mixed calibration set kernels. The
203 mixed calibration set kernels were comprised of seven uninoculated, seven asymptomatic, seven
204 mildly damaged and ten severely damaged kernels arranged randomly as shown in Figure 6A. The
205 reflectance image of a selected channel of these kernels is shown in Figure 6B. The background
206 noise was removed by using the mask shown in Figure 6C. *Fusarium*-damaged/ DON
207 contaminated regions (depicted by red pixels) and healthy/ DON free regions (depicted by green
208 pixels) of each kernel were predicted using PLSR and LDA (Figure 6D). The severely damaged
209 kernels were dominated by red pixels while the uninoculated and asymptomatic kernels were
210 dominated by green pixels showing that HSI can successfully detect level of *Fusarium*-damage.
211 This observation is clearly shown by the differences in the mean percentage of damaged pixels in
212 the calibration images of each kernel category (Table 2).

213 *Figure 6 comes here.*

214 Figure 7 shows the PLS-LDA classification model used for classification of individual
215 pixels in the eight validation images. There was a clear difference between classes, as indicated by
216 the extent of red and green pixels and by the differences among the mean percentage of damaged
217 pixels in the validation images of each kernel category. (Figure 7 and Table 2). Hyperspectral

imaging detected *Fusarium* damage and DON level more precisely than visual examination. Kernels with very high DON but categorized as mildly damaged were dominated by infected regions. On the other hand, kernels with very low DON but categorized as severely damaged were dominated by healthy regions after image analysis (Figure 7).

Figure 7 comes here.

Table 2 comes here.

The DON* value for the 112 validation set kernels ((4 dorsal + 4 ventral images) x 14 kernels representing each kernel category) were predicted in two alternative ways: 1) using the average spectrum of the kernels as x-variables and the PLSR model, and 2) classifying every pixel using the PLS-LDA model, and calculating the ratio of damaged pixels in each grain. . The correlation (R) between predicted and measured DON* values were 0.81 and 0.79 respectively (Figure 8). The difference between the two prediction methods is not statistically significant, showing that they are equivalent. Both methods indicate a valid model showing a good potential of HSI in detecting *Fusarium* damage and predicting DON in oats.

Figure 8 comes here.

CONCLUSIONS

Hyperspectral images of individual oat kernels with different levels of *Fusarium* damage and DON content were analysed. Hyperspectral imaging successfully detected *Fusarium* damage of kernels with better accuracy than visual inspection. Detection of *Fusarium* damage with HSI gave a better indication of DON content of kernels than visual assessment of damage. Regions within single kernels were further classified as *Fusarium*-damaged and healthy regions. A PLSR

model was developed using the transformed DON* values as y-variables and the average spectra of each kernel as x-variables. The model was proved to be valid and stable by detecting DON* values of a set of separate validation kernels. The results reported in this paper indicate that HSI can successfully be implemented to detect *Fusarium* damage and DON contamination in single oat kernels. Thus, highly damaged and contaminated kernels can be detected and removed to significantly lower toxin contamination and improve grain quality of seed lots. Kernels used in this paper are of a single oat genotype originating from a single experimental year. Testing the feasibility of HSI to detect *Fusarium* damage and DON contamination in several genotypes across experimental years would be an important step towards the routine application of the method for screening purposes.

ACKNOWLEDGEMENTS

We acknowledge the financial support of the Norwegian Research Council and Graminor AS to the project 'Mycotoxin contamination in Norwegian food and feed: Modelling reductive approaches and risk assessment with regards to the whole food chain (Project number 19412)'. We thank Dr. Yanhong Dong (Department of Plant Pathology, University of Minnesota) for DON analysis, Elin Ørmen (Imaging Center, Norwegian University of Life Sciences) for her help in microscopy and Andreas Flø (Institute of Mathematics and Technology, Norwegian University of Life Sciences) for his help in hyperspectral imaging.

LITERATURE CITED

Bechtel, D. B., Kaleikau, L. A., Gaines, R. L., Seitz, L. M. 1985. The effects of *Fusarium graminearum* infection on wheat kernels. Cereal Chem. 62: 191-7.

Bergsjø, B., Langseth, W., Nafstad, I., Jansen, J. H., Larsen, H. J. S. 1993. The effects of naturally deoxynivalenol contaminated oats on the clinical condition, blood parameter, performance and carcass composition of growing pigs. Vet. Res. Commun. 17: 283-94.

Bernhoft, A., Eriksen, G. S., Sundheim, L., et al., 2013. Risk assessment of mycotoxins in cereal grain in Norway: Opinion of the Scientific Steering Committee of the Norwegian Scientific Committee for Food Safety. In.: Norwegian Scientific Committee for Food Safety (VKM).

Bottalico, A., Perrone, G. 2002. Toxigenic *Fusarium* species and mycotoxins associated with head blight in small-grain cereals in Europe. Eur. J. Plant Pathol. 108: 611-24.

D'mello, J. P. F., Placinta, C. M., Macdonald, A. M. C. 1999. *Fusarium* mycotoxins: a review of global implications for animal health, welfare and productivity. Anim. Feed Sci.Technol. 80: 183-205.

Delwiche, S. R., Kim, M. S., Dong, Y. 2011. *Fusarium* damage assessment in wheat kernels by Vis/NIR hyperspectral imaging. Sensory and Instrumentation for Food Quality 5: 63-71.

Dexter, J. E., Clear, R. M., Preston, K. R. 1996. Fusarium head blight: effect on the milling and baking of some Canadian wheats. Cereal Chem. 73: 695-701.

Feng, Y. Z., Sun, D. W. 2012. Application of hyperspectral imaging in food safety inspection and control: a review. Critical Reviews in Food Science and Nutrition 52: 1039-58

Gowen, A. A., O'donnell, C. P., Cullen, P. J., Downey, G., Frias, J. M. 2007. Hyperspectral imaging- an emerging process analytical tool for food quality and safety control. Trends Food Sci. Tech. 18: 590-8.

Jackowiak, H., Packa, D., Wiwart, M., Perkowski, J. 2005. Scanning electron microscopy of *Fusarium* damaged kernels of spring wheat. Int. J. Food Microbiol. 98: 113- 23.

Jiang, G., Dong, Y., Lewis, J. M., Siler, L., Ward, R. R., 2006. Characterization of resistance to *Fusarium graminearum* in a recombinant inbred line population of wheat: resistance to fungal spread, mycotoxin accumulation, and grain yield loss, and trait relationship. Crop Sci. 46: 2590 - 7.

Langevin, F., Eudes, F., Comeau, A. 2004. Effect of trichothecenes produced by *Fusarium graminearum* during Fusarium head blight development in six cereal species. Eur. J. Plant Pathol. 110: 735-46.

Liu, W., Langseth, W., Skinnes, H., Elen, O. N., Sundheim, L. 1997. Comparison of visual head blight ratings, seed infection levels, and deoxynivalenol production for assessment of resistance in cereals inoculated with *Fusarium culmorum*. Eur. J. Plant Pathol. 103: 589-95.

Mcmullen, M., Jones, R., Gallenberg, D. 1997. Scab of wheat and Barley: a re-emerging disease of devastating impact. Plant Dis. 81: 1340-8.

Nightingale, M. J., Marchylo, B. A., Clear, R. M., Dexter, J. E., Preston, K. R. 1999. Fusarium head blight: effect of fungal proteases on wheat storage proteins. Cereal Chem. 76: 150-8.

Parry, D. W., Jenkinson, P., Mcleod, L. 1995. Fusarium ear blight (scab) in small grain cereals—a review. Plant Pathology 44: 207-38.

Polder, G., Heijden, G.W. M. V. D, Waalwijk, C., Young, I. T. 2005. Detection of *Fusarium* in single wheat kernels using spectral imaging. Seed Science and Technology 33: 655-68.

Schwarz, P. B., Schwarz, J. G., Zho, A., Prom, L. K., Steffenson, B. J. 2001. Effect of *Fusarium graminearum* and *F. poae* infection on barley and malt quality. Monatsschrift Fur Brauwissenschaft 314: 55-63.

304 Shahin, M. A., Symons, S. J. 2011. Detection of *Fusarium* damaged kernels in Canada Western
305 Red Spring wheat using visible/near-infrared hyperspectral imaging and principal
306 component analysis. Computers and Electronics in Agriculture 75: 107-12.
307 Shahin, M. A., Symons, S. J. 2012. Detection of *Fusarium* damage in Canadian wheat using
308 visible/near-infrared hyperspectral imaging. Food Measure 6: 3-11.
309 Siuda, R., Balcerowska, G., Kupcewicz, B., Lenc, L. 2008. A modified approach to evaluation of
310 DON content in scab-damaged ground wheat by use of diffuse reflectance spectroscopy.
311 Food Anal. Methods 1: 283-92.
312 Snijders, C. H. A., Perkowski, J. 1990. Effects of head blight caused by *Fusarium culmorum* on
313 toxin content and weight of wheat kernels. Phytopathology 80: 566-70.
314 Tekle, S., Bjørnstad, Å., Skinnes, H., Dong, Y., Segtnan, V. H. 2013. Estimating deoxynivalenol
315 content of ground oats using VIS-NIR spectroscopy. Cereal Chem. 90: 181–185
316 Wang, J., Pawelzik, E., Weinert, J., Wolf, G. A., 2005. Impact of *Fusarium culmorum* on the
317 polysaccharides of wheat flour. J. Agric. Food Chem. 53: 5818-23.
318 Williams, P., Manley, M., Fox, G., Geladi, P. 2010. Indirect detection of *Fusarium verticillioides*
319 in maize (*Zea mays* L.) kernels by near infrared hyperspectral imaging. J. Near Infrared
320 Spectrosc. 18: 49-58.
321

322 Table 1: Mean (± standard deviation), minimum and maximum kernel weight (g) and
323 deoxynivalenol content (ppm) of calibration (*n*=31) and validation (*n*=14) set samples of
324 asymptomatic (A), mildly damaged (MD), severely damaged (SD) and uninoculated (U) kernels.
325 'nd' stands for non-detectable level of DON (< 5 ng/ sample).

		Calibration set		Validation set	
		Kernel weight (g)	DON (ppm)	Kernel weight (g)	DON (ppm)
	A	0.054 ± 0.005	1.93 ± 4.49	0.056 ± 0.005	4.99 ± 7.83
	MD	0.048 ± 0.008	25.31 ± 53.94	0.046 ± 0.010	56.82 ± 107.43
	SD	0.036 ± 0.009	136.34 ± 123.04	0.032 ± 0.008	117.61 ± 107.25
Mean	U	0.050 ± 0.013	0.09 ± 0.05	0.045 ± 0.008	0.01 ± 0.05
	A	0.045	nd	0.051	0.18
	MD	0.034	nd	0.029	nd
	SD	0.019	0.48	0.018	0.52
Minimum	U	0.033	nd	0.034	nd
	A	0.062	20.50	0.064	21.91
	MD	0.061	267.37	0.061	355.32
	SD	0.056	386.51	0.048	340.10
Maximum	U	0.062	0.66	0.058	0.18

326

327

328 Table 2 Mean (± standard deviation) percentage of damaged pixels in uninoculated, asymptomatic,
329 mildly damaged and severely damaged kernels of the calibration (*n*= 248) and validation (*n*=112)
330 images. Ventral and dorsal images were pooled for each kernel category.

	Uninoculated	Asymptomatic	Mildly Damaged	Severely Damaged
Calibration set	21.5 ± 5.4	28.1 ± 8.0	39.8 ± 12.9	62.8 ± 16.4
Validation set	26.5 ± 7.4	29.3 ± 7.1	46.9 ± 18.4	73.3 ± 16.3

331

332

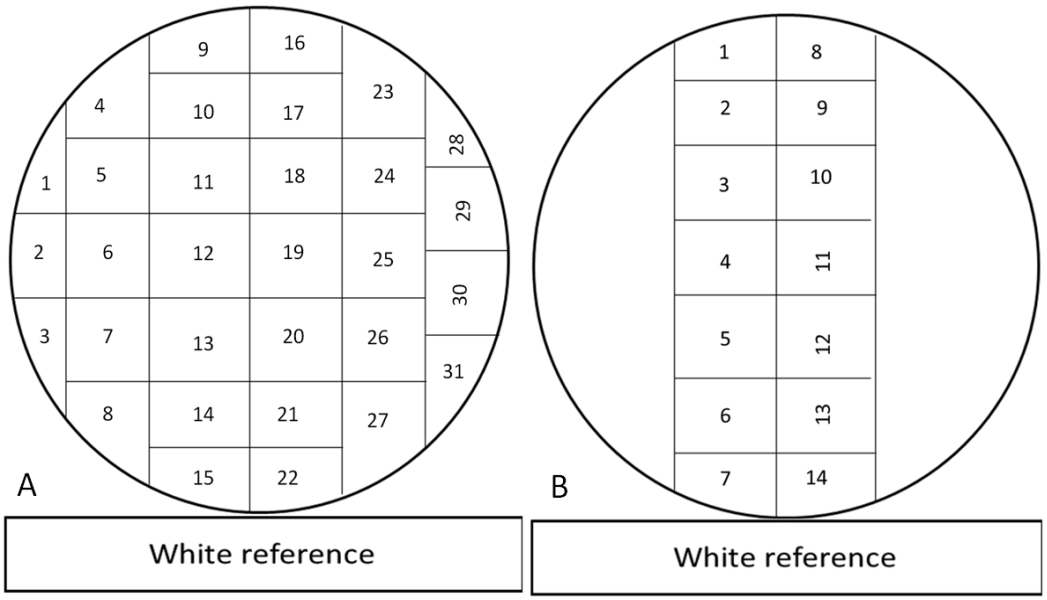

Figure 1: Presentation of kernels for hyperspectral imaging. Ventral and dorsal surfaces of 31 test set kernels (A) and the 14 validation set kernels (B) from each kernel category were scanned. Numbers in the cells represent kernel numbers. Kernels were scanned with their basal portions towards the white reference. Kernels 28, 29, and 30 in the calibration set and kernels 11, 12 and 13 in the validation set were rotated 90^{o} to serve as signposts.

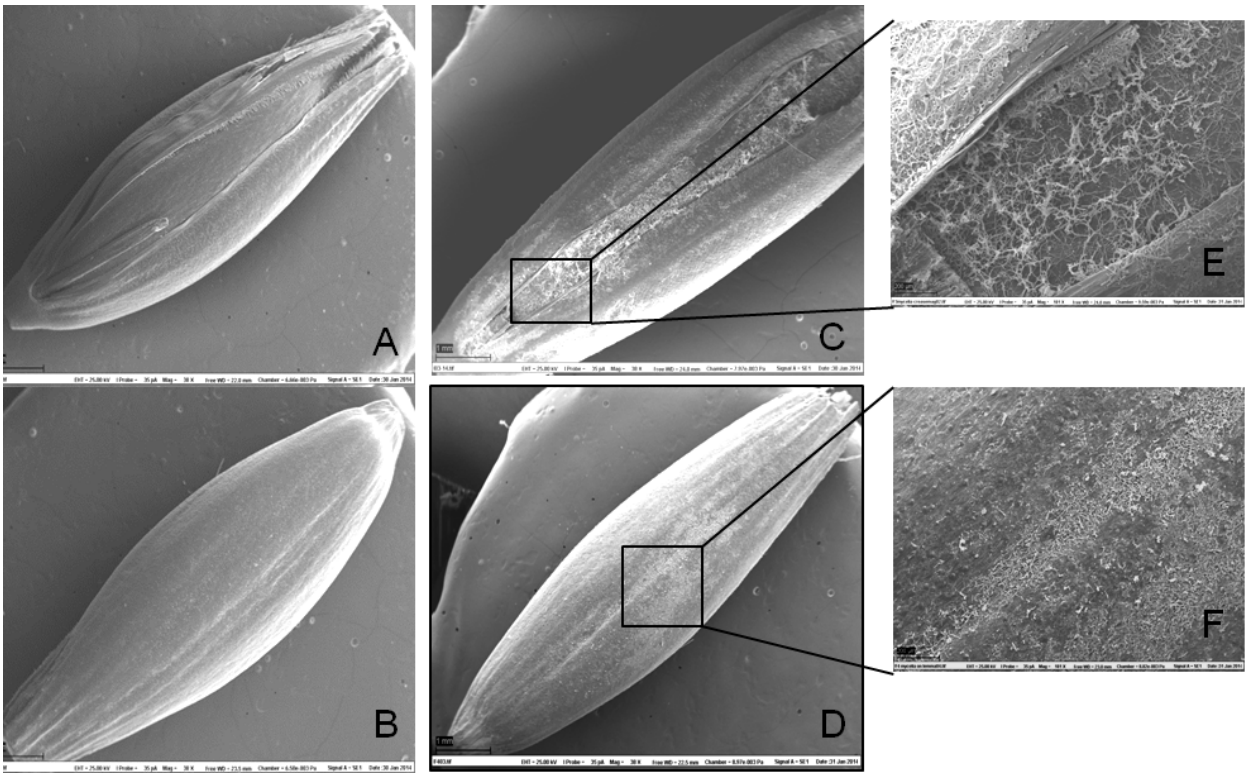

Figure 2: Scanning electron micrographs of ventral and dorsal surfaces of hulled kernels of healthy (A and B, magnification = 38 x) and *Fusarium*-damaged (C and D, magnification= 38x) kernels of the oat cv. Bessin. Higher magnification reveals profuse growth of *F. graminearum* mycelia in the crease on the palea (E, magnification= 181x) and on the lemma (F, magnification= 181x).

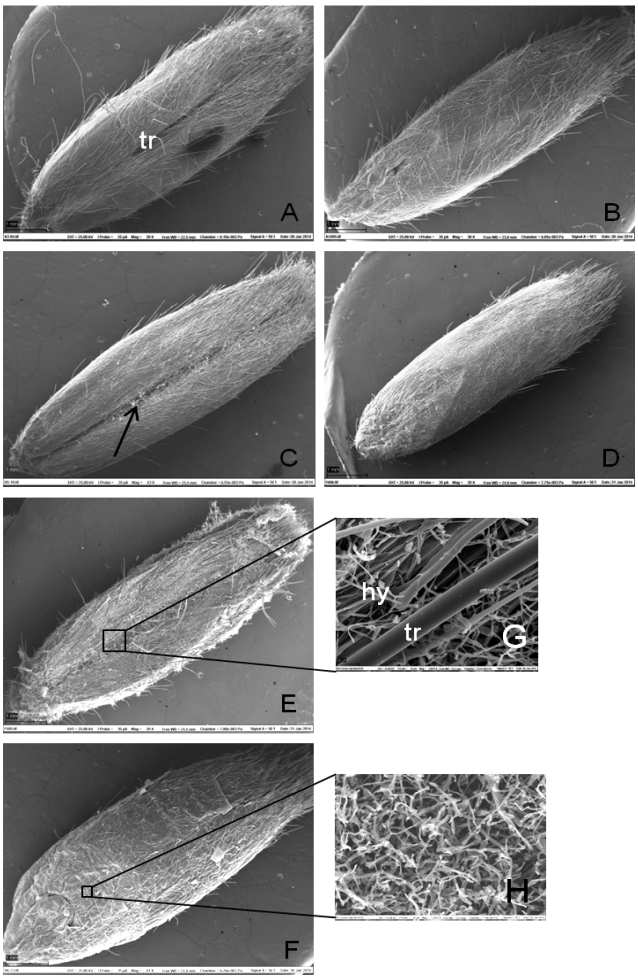

Figure 3: Scanning electron micrographs of ventral and dorsal surfaces of dehulled kernels of the oat cv. Bessin. A and B show well-formed mycelium on ventral (A, magnification= 39x) and dorsal (B, magnification= 38x) surfaces of healthy kernels, with the trichomes (tr). C and D show ventral (C, magnification= 43x) and dorsal (D, magnification= 39x) surfaces of mildly damaged kernels, arrow indicates mycelia of *Fusarium graminearum*. E and F are micrographs of ventral (E, magnification= 39x) and dorsal (F, magnification= 41x) surfaces of severely damaged kernels. G and H are higher magnifications of fungal growth on the ventral (G, magnification= 1.6kx, hy= hyphae, and tr= trichome) and dorsal surfaces (H, magnification= 1.46kx).

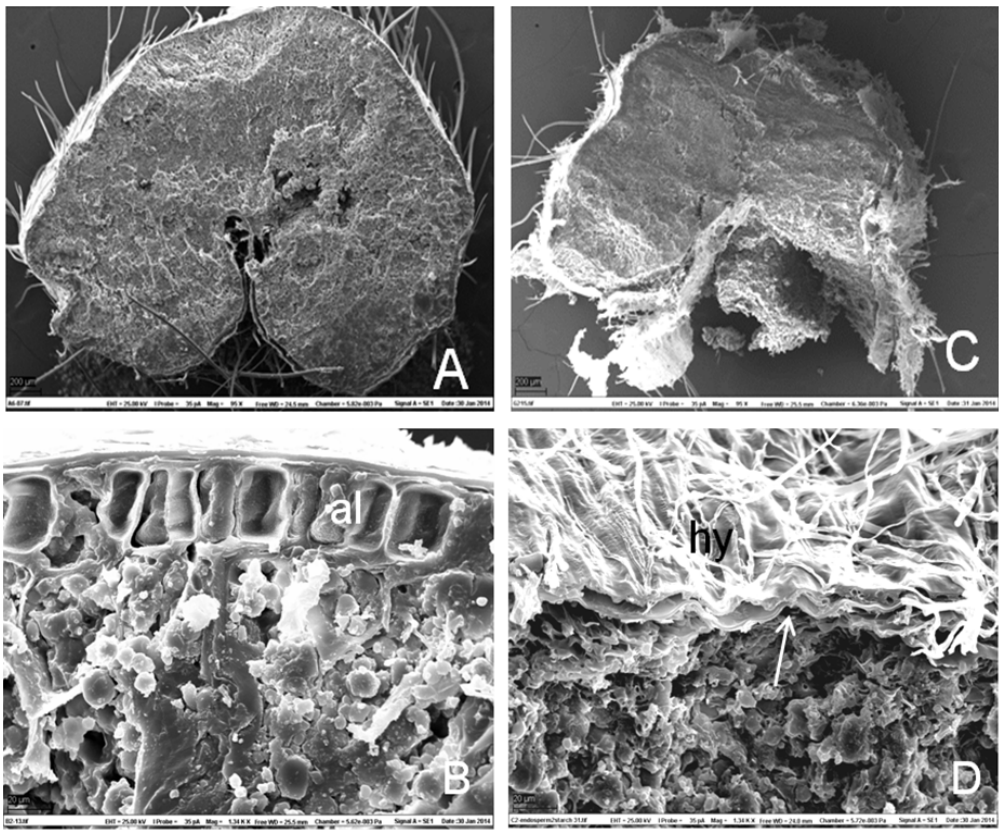

Figure 4: Scanning electron micrographs of cross sections of healthy (A, magnification= 95x; and B, magnification= 1.34 kx) and *Fusarium*-damaged (C, magnification= 95x; and D, magnification= 1,34 kx) kernels of the oat cv. Bessin. A well formed aleurone layer (al) and endosperm with small and large starch granules in the protein matrix of the healthy kernel is displayed in B. Hyphae (hy) of *Fusarium graminearum* and collapsed aleurone layer and damaged endosperm are shown in D.

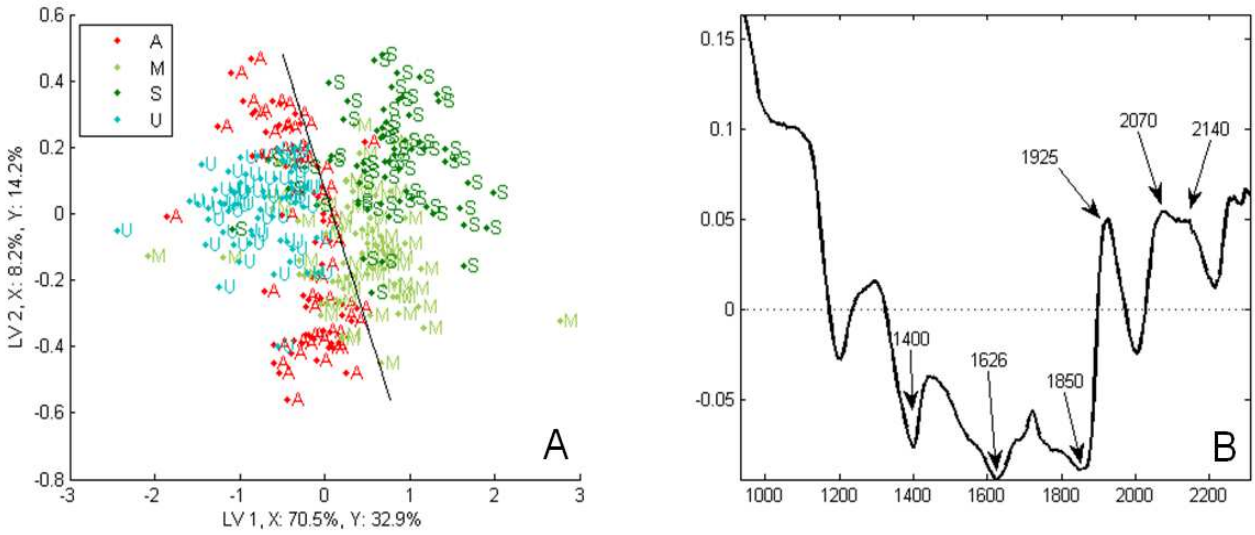

363

364 Figure 5: Partial least squares (PLS) regression on the calibration set kernels with the average
365 spectra of kernels as X variables and DON*= [log(DON)]^3 values as Y variables. (A) PLS scores
366 of calibration set kernels on component 1 versus component 2, with separation line from linear
367 discriminant analysis. A- asymptomatic, M- mildly damaged, S- severely damaged and U-
368 uninoculated kernels. (B) PLS loading weights from the first component. Wavelengths of interest
369 are marked by arrows.

370

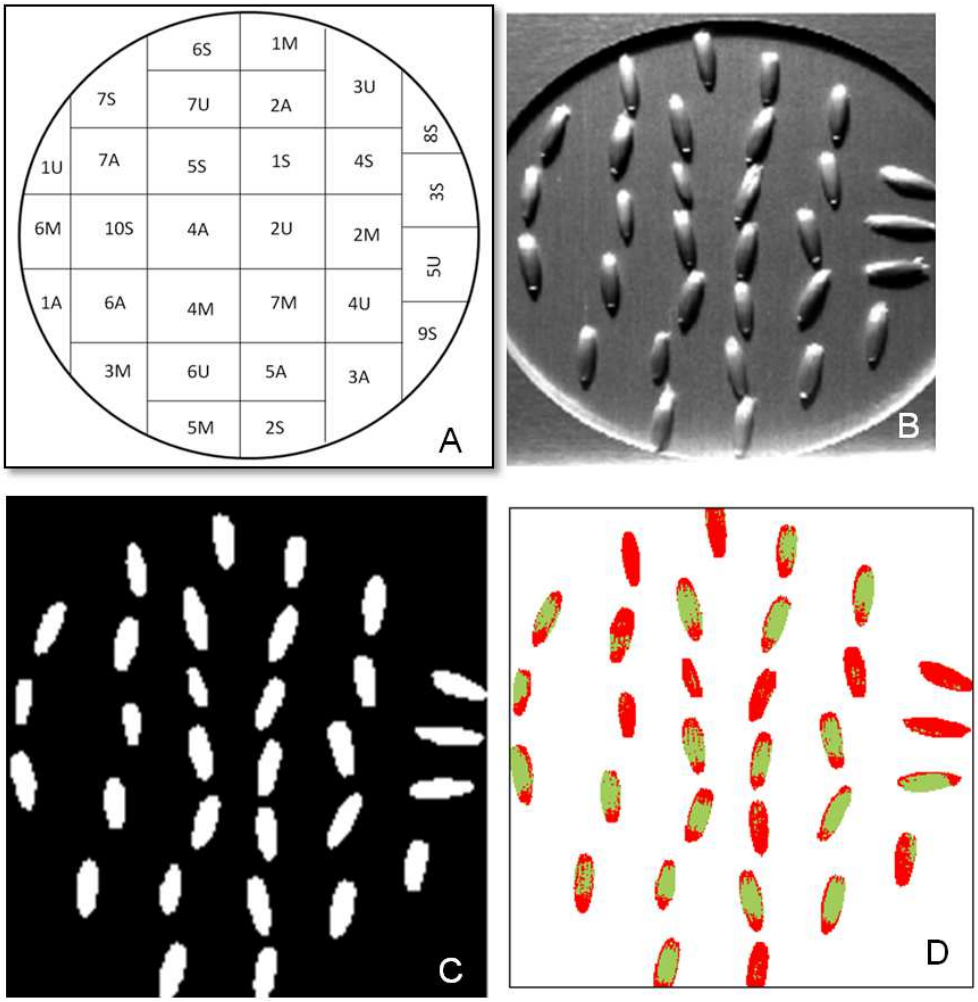

Figure 6: Image analysis of calibration set kernels comprising seven uninoculated, seven asymptomatic, seven mildly damaged and ten severely damaged kernels. (A) Sample presentation for scanning. Numbers represent the kernel number in the original calibration set and letters represent kernel category. A- asymptomatic, M- mildly damaged, S- severely damaged and U-uninoculated kernels. (B) Reflectance spectra of one selected channel. (C) Mask used to remove background from images. D) Image showing infection in grains. Red pixels represent DON-contaminated/ *Fusarium*-damaged areas and green pixels represent DON-free/ healthy areas.

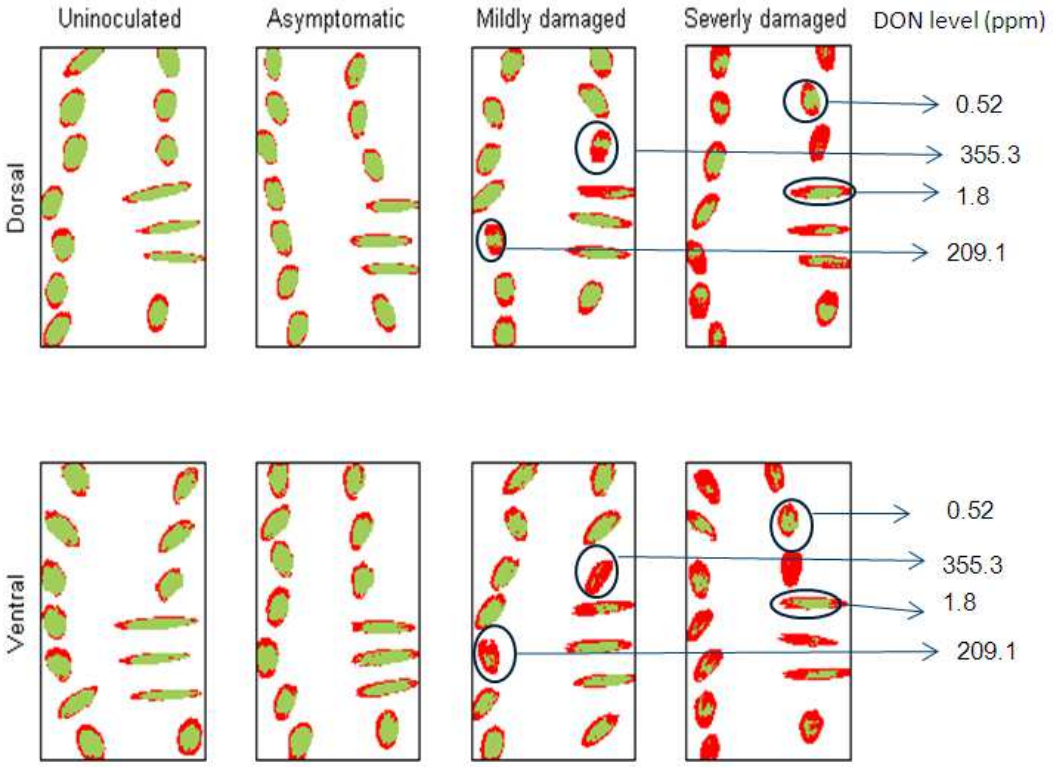

379

380 Figure 7: Classification of pixels in validation images. *Fusarium*-damaged/ DON-contaminated
381 areas are depicted in red while healthy/ DON-free areas are depicted in green. DON values of
382 kernels of interest (kernels with relatively high DON level in the mildly damaged category and
383 kernels with low DON level in the severely damaged category) are shown.

384

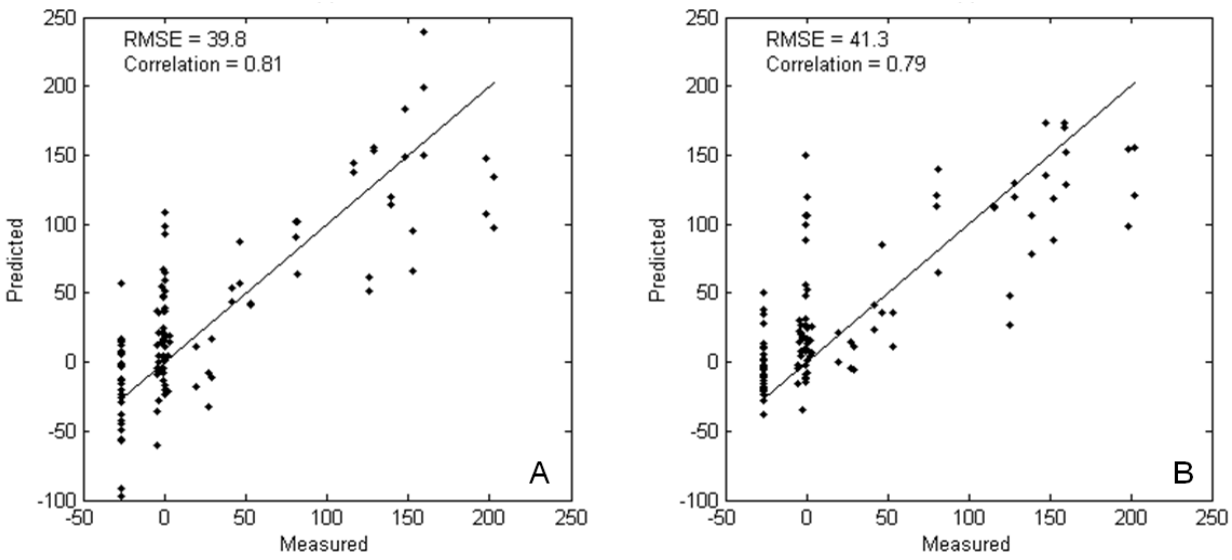

385

386 Figure 8: Measured versus predicted DON*= [log(DON)]^3 values of validation kernels using the
387 partial least squares (PLS) regression model developed (A) and the PLS- linear discriminant
388 analysis model (B).

389